In particular, if, for a suitable choice of the reference planes of the junction, we assume $\phi_1 = 0$, we can write the set of eigenvalues as follows:

$$\left.\begin{aligned} s_1 &= e^{-\alpha_1} \\ s_2 &= \exp\left[-\alpha_2 + j\left(\frac{-2\pi}{3} + \delta_2\right)\right] \\ s_3 &= \exp\left[-\alpha_3 + j\left(\frac{2\pi}{3} + \delta_3\right)\right] \end{aligned}\right\} \alpha_i \geqq 0 \ (i = 1, 2, 3). \quad (24)$$

In this description of the imperfect circulator, no element has been included that could alter the symmetry of the junction and therefore all the properties enumerated earlier in points 1)–4) still apply. In particular, the property expressed in point 4) will remain valid. By utilizing the relationships (16)–(18) when the eigenvalues are given by (24), one obtains for the elements of $\mathbf{S}^{(f)}$ the following relationships:

$$\begin{aligned} S' &= \frac{1}{3}\left\{e^{-\alpha_1} - \frac{1}{2}\left(e^{-\alpha_3 + j\delta_3} + e^{-\alpha_2 + j\delta_2}\right) + j\frac{\sqrt{3}}{2}\left(e^{-\alpha_3 + j\delta_3} - e^{-\alpha_2 + j\delta_2}\right)\right\} \\ S'' &= \frac{1}{3}\left\{e^{-\alpha_1} + e^{-\alpha_2 + j\delta_2} + e^{-\alpha_3 + j\delta_3}\right\} \\ S''' &= \frac{1}{3}\left\{e^{-\alpha_1} - \frac{1}{2}\left(e^{-\alpha_3 + j\delta_3} + e^{-\alpha_2 + j\delta_2}\right) - j\frac{\sqrt{3}}{2}\left(e^{-\alpha_3 + j\delta_3} - e^{-\alpha_2 + j\delta_2}\right)\right\}. \end{aligned} \quad (25)$$

If the α_i and the δ_i are small, we obtain, by expanding the exponentials in series,

$$\begin{aligned} S' &\cong \frac{1}{3}\left\{\left[-\alpha_1 + \frac{1}{2}(\alpha_3 + \alpha_2) - \frac{\sqrt{3}}{2}(\delta_3 - \delta_2)\right] - j\frac{1}{2}\left[\delta_3 + \delta_2 + \sqrt{3}(\alpha_3 - \alpha_2)\right]\right\} \\ S'' &= \frac{1}{3}\left\{[3 - (\alpha_1 + \alpha_2 + \alpha_3)] + j[\delta_2 + \delta_3]\right\} \\ S''' &\cong \frac{1}{3}\left\{\left[-\alpha_1 + \frac{1}{2}(\alpha_3 + \alpha_2) + \frac{\sqrt{3}}{2}(\delta_3 - \delta_2)\right] - j\frac{1}{2}\left[\delta_3 + \delta_2 - \sqrt{3}(\alpha_3 - \alpha_2)\right]\right\}. \end{aligned} \quad (26)$$

By the inspection of (25) and (26), and remembering that $|S'|^2$, $|S''|^2$, and $|S'''|^2$ correspond respectively to the power reflected at the input arm, the power transmitted at the forward arm, the power transmitted at the isolated arm, one derives the following observations: 1) for a lossless circulator, affected by small values of δ_2 and δ_3, $|\delta'|^2 = |S'''|^2$, *i.e.*, the power appearing at the isolated arm equals the power reflected at the input arm; 2) for a lossy circulator, in the general case $|S'|^2 \neq |S'''|^2$ even for small values of the α_i and δ_i ($i = 1, 2, 3$) and for suitable combinations of these last quantities, the ratio $|S'|^2/|S'''|^2$ can be quite different from unity.

ACKNOWLEDGMENT

The authors are greatly indebted to Dr. M. H. Sirvetz for his helpful advice and his continued interest in this work. Appreciation is also expressed for the technical assistance of J. Matsinger during the execution of the experimental measurements.

A Wide-Band UHF Traveling-Wave Variable Reactance Amplifier*

R. C. HONEY† AND E. M. T. JONES†

Summary—The techniques developed for designing periodically loaded traveling-wave parametric amplifiers using variable-reactance diodes are described in detail. An amplifier was built and tested with two different sets of eight diodes. The performance of the amplifier with each set of diodes agrees substantially with the theoretical predictions, the measured noise figures being about 1.2 db higher than the theoretical values in each case. The gain of the second amplifier varied from a minimum of 6.7 db to more than 13 db over the band from 550 to 930 mc, with a measured noise figure of 2.3 db for wide-band noise inputs in the middle of the band, corresponding to about 4.9 db for single-frequency inputs.

* Manuscript received by the PGMTT, December 7, 1959; revised manuscript received, January 28, 1960.
† Stanford Research Institute, Menlo Park, Calif.

GENERAL

TRAVELING-WAVE parametric amplifiers have a number of useful properties, such as wide bandwidth and unilateral amplification, that have been thoroughly discussed in the rapidly expanding litera-

ture on this subject.[1–21] The detailed design procedure and the preliminary experimental results on one such amplifier are reported here; a schematic diagram of the amplifier is shown in Fig. 1. This amplifier uses eight variable-reactance diodes periodically loading a uniform high-impedance TEM transmission line. As shown in Fig. 1, this line propagates both the signal and the idling frequencies. An inductive reactance consisting of a suitable length of short-circuited transmission line is connected across each diode, forming a parallel resonant circuit whose resonant frequency is adjusted to fall within the first pass band of the periodically loaded line.

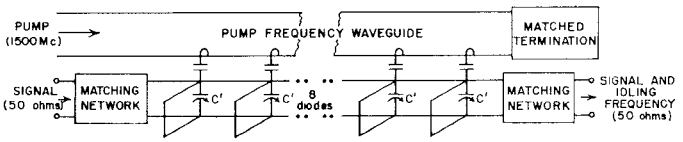

Fig. 1—Traveling-wave parametric amplifier.

[1] R. Adler, "A New Principle of Signal Amplification," presented at the Conf. on Electron Tube Research, Berkeley, Calif.; June, 1957.
[2] Y. Miyakawa, "Amplification and frequency conversion in propagating circuits," *Inst. Elec. Comm. Engrs. Japan Natl. Conv. Record*, p. 8; November, 1957. (In Japanese.)
[3] A. L. Cullen, "A traveling-wave parametric amplifier," *Nature*, vol. 181, p. 332; February 1, 1958.
[4] P. K. Tien and H. Suhl, "A traveling-wave ferromagnetic amplifier," PROC. IRE, vol. 46, pp. 700–706; April, 1958.
[5] W. H. Louisell and C. F. Quate, "Parametric amplification of space charge waves," PROC. IRE, vol. 46, pp. 707–716; April, 1958.
[6] A. Uhlir, Jr., "The potential of semiconductor diodes in high-frequency communications," PROC. IRE, vol. 46, p. 1099; June, 1958.
[7] R. Adler, "Parametric amplification of the fast electron wave," PROC. IRE, vol. 46, pp. 1300–1301; June, 1958.
[8] L. D. Buchmiller and G. Wade, "Pumping to extend traveling-wave tube frequency range," PROC. IRE, vol. 46, pp. 1420–1421; July, 1958.
[9] P. K. Tien, "Parametric amplification and frequency mixing in propagating circuits," *J. Appl. Phys.*, vol. 29, pp. 1347–1357; September, 1958.
[10] R. S. Engelbrecht, "A low-noise nonlinear reactance traveling-wave amplifier," PROC. IRE, vol. 46, p. 1655; September, 1958.
[11] R. Adler, G. Hrbek, and G. Wade, "A low-noise electron-beam parametric amplifier," PROC. IRE, vol. 46, pp. 1756–1757; October, 1958.
[12] A. Ashkin, "Parametric amplification of space charge waves," *J. Appl. Phys.*, vol. 29, pp. 1646–1651; December, 1958.
[13] G. Wade and R. Adler, "A new method for pumping a fast space-charge wave," PROC. IRE, vol. 47, pp. 79–80; January, 1959.
[14] W. E. Danielson, "Low noise in solid state parametric amplifiers at microwave frequencies," *J. Appl. Phys.*, vol. 30, pp. 8–15; January, 1959.
[15] R. S. Engelbrecht, "Nonlinear-Reactance Traveling-Wave Amplifiers for UHF," presented at Solid-State Circuits Conf., Philadelphia, Pa.; February, 1959.
[16] L. S. Nergaard, "Nonlinear-capacitance amplifiers," *RCA Rev.*, vol. 20, pp. 3–17; March, 1959.
[17] P. P. Lombardo and E. W. Sard, "Low-frequency prototype traveling-wave reactance amplifier," PROC. IRE, vol. 47, pp. 995–996; May, 1959.
[18] G. M. Roe and M. R. Boyd, "Parametric energy conversion in distributed systems," PROC. IRE, vol. 47, pp. 1213–1218; July, 1959.
[19] K. Kurokawa and J. Hamaski, "Mode theory of lossless periodically distributed parametric amplifiers," IRE TRANS. ON MICROWAVE THEORY AND TECHNIQUES, vol. MTT-7, pp. 360–365; July, 1959.
[20] P. P. Lombardo and E. W. Sard, "Low-noise microwave reactance amplifiers with large gain-bandwidth products," 1959 IRE WESCON CONVENTION RECORD, pt. 1, pp. 83–98.
[21] C. V. Bell and G. Wade, "Circuit considerations in traveling-wave parametric amplifiers," 1959 IRE WESCON CONVENTION RECORD, pt. 2, pp. 75–82.

The pump frequency at 1500 mc is carried by a waveguide paralleling the TEM transmission line, and coupled loosely to each diode with loop coupling from the waveguide and capacitive coupling to the TEM line. The characteristics of the periodically loaded TEM line are chosen so that the pump frequency is in a stopband of the line. The upper sideband, at the signal frequency plus the pump frequency, is either in a stopband or is grossly out of phase for all signal frequencies, so that it cannot affect the interaction appreciably. Similarly, the signal and idling frequencies cannot propagate along the pump channel since they are below the cutoff frequency of the pump waveguide. The matching networks shown in the figure transform the high image impedance of the amplifier to an approximate 50-ohm level for use with conventional coaxial instrumentation.

Analysis and Design

General

In a periodically loaded transmission structure such as this, the conditions that must be satisfied to permit parametric interaction between the signal frequency and the pump frequency are given by

$$\omega_1 + \omega_2 = \omega_3, \tag{1}$$

$$\beta_1 + \beta_2 \approx \beta_3 \pm 2n\pi, \tag{2}$$

where

$n = 0, 1, 2, \cdots$
$\omega_1 = 2\pi f_1$, radians per second
f_1 = signal frequency, cycles per second
$\omega_2 = 2\pi f_2$, radians per second
f_2 = idling frequency, cycles per second
$\omega_3 = 2\omega f_3$, radians per second
f_3 = pump frequency, cycles per second
$\beta_m = \omega_m / v_m (m = 1, 2, 3)$
v_m = phase velocity of mth frequency along the loaded transmission line.

The idling frequency, ω_2, is generated by the variable capacitors so as to satisfy (1) exactly. However, (2) need be satisfied only approximately, since the gain of the amplifier is not greatly reduced if the phase error is small.[4]

The maximum gain for such an amplifier is given approximately by[21]

$$\alpha = (\omega_1\omega_2)^{1/2}(Z_{\pi 1}Z_{\pi 2})^{1/2}\Delta C/4 \text{ nepers per section}$$

$$= 13.65 Z_0 (f_1 f_2)^{1/2} \left(\frac{Z_{\pi 1}}{Z_0} \cdot \frac{Z_{\pi 2}}{Z_0}\right)^{1/2} \Delta C \text{ db per section} \tag{3}$$

where

ΔC = one-half the peak-to-peak capacitance variation ($C' = C + \Delta C \cos \omega_3 t$) in farads
C = average capacitance in farads
C' = total instantaneous capacitance in farads

$Z_{\pi 1}$ = image impedance in ohms of loaded line as seen by each diode at ω_1

$Z_{\pi 2}$ = image impedance in ohms of loaded line as seen by each diode at ω_2

Z_0 = characteristic impedance in ohms of uniform line.

This equation contains the most important factors which must be considered in the design of a traveling-wave parametric amplifier.

The following subsections will discuss in detail the analysis and design of circuits satisfying (1) and (2), methods for maximizing the gain in (3), and the design of the matching sections at each end of the amplifier.

Image Parameters of Periodically-Loaded Lines

When any transmission structure is shunt-loaded with variable-reactance diodes, the gain of the amplifier becomes proportional to the square root of the product of the image impedances of the structure at the signal and idling frequencies as seen at the terminals across which the diodes are connected, as given by (3). It turns out that the image impedance of a uniform transmission line with periodic shunt reactive elements of any type assumes a particularly simple form, and a knowledge of the phase velocity along the structure as a function of frequency, such as contained in the conventional ω vs β curve for that structure, is sufficient to predict immediately the image impedance of the structure. This can be shown in the following way. Assume that a uniform transmission system of characteristic admittance, Y_0, is periodically loaded with shunt susceptances, $j2B$, as shown in Fig. 2(a). Let the phase constant of the unloaded line be β_0, or $\beta_0 = 2\pi/\lambda = \omega/v$, where ω is the angular frequency, v the velocity of light in the medium, and λ the wavelength on the uniform transmission line. A typical half section of this line is shown in Fig. 2(b), for which the image phase constant, ϕ, in radians per section, can be found from either

$$\tanh \frac{\phi}{2} = \sqrt{\frac{Y_{oc}}{Y_{sc}}}, \tag{4}$$

or

$$\cosh \phi = \frac{Y_{sc} + Y_{oc}}{Y_{sc} - Y_{oc}}, \tag{5}$$

where

Y_{sc} = input admittance when opposite terminal-pair is short circuited

Y_{oc} = input admittance when opposite terminal-pair is open circuited.

The image admittances, Y_π and Y_T, are also found from the usual formula

$$Y_{\pi,T} = \sqrt{Y_{oc} Y_{sc}}. \tag{6}$$

The open- and short-circuit admittances for the left-hand terminal pair of the half section shown in Fig. 2(b) are given by

$$Y_{oc} = jB + jY_0 \tan (\beta_0 L/2)$$
$$Y_{sc} = jB - jY_0 \cot (\beta_0 L/2). \tag{7}$$

Hence, from (5),

$$\frac{B}{Y_0} = \frac{\cos \beta_0 L - \cos \beta L}{\sin \beta_0 L}, \tag{8}$$

where $\phi = j\beta L$ in the pass bands of the structure.

Finally, the π-section image admittance at the left-hand terminal pair Y_π, found by combining (6) to (8), reduces to the simple equation

$$\frac{Y_\pi}{Y_0} = \frac{\sin \beta L}{\sin \beta_0 L} \quad \text{or} \quad \frac{Z_\pi}{Z_0} = \frac{\sin \beta_0 L}{\sin \beta L}. \tag{9}$$

Eq. (9) can be plotted on an ω vs β diagram as shown in Fig. 3, forming an auxiliary grid of lines which are labeled with the constant values of Z_π/Z_0 along each line. Hence, if the ω vs β curve of any periodically shunt-

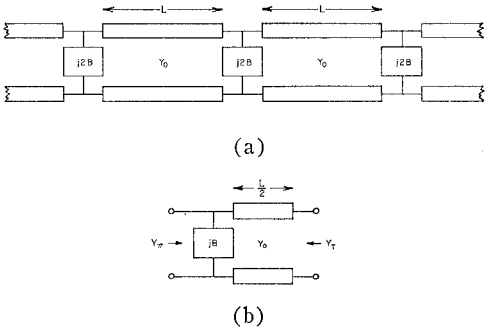

Fig. 2—Notation for periodically loaded transmission lines. (a) Periodically loaded transmission line. (b) Typical half section.

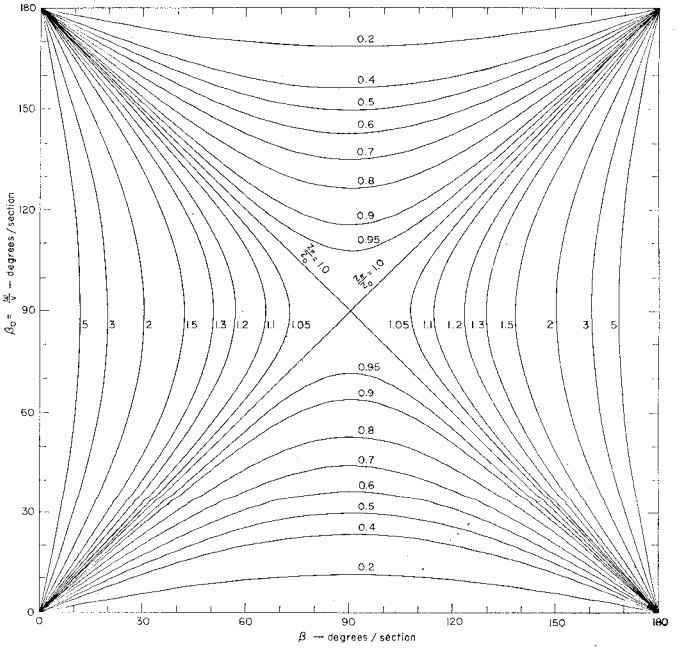

Fig. 3—Image impedances for periodic shunt-loaded transmission line.

loaded nondispersive transmission line is superimposed on this grid, the image impedances can be read directly from the intersections of the curve with the grid lines. This is true regardless of the nature of the reactive shunt loading. Since the gain of a parametric amplifier of the type considered here is proportional to the square root of the product of the image impedances at the signal and idling frequencies, it becomes a simple matter to compare the gains of two circuits of this type from their respective ω vs β curves, other factors being constant.

A study of Fig. 3 shows that maximum image impedances are obtained in circuits whose ω vs β curves pass through the center of the figure at $\beta_0 = \omega/v = \beta = 90$ degrees per section.

Periodic Structure Used in Amplifier

The actual structure chosen for use in the traveling-wave parametric amplifier described here is shown in Fig. 1, and uses a length of shorted transmission line of characteristic impedance Z_0 in parallel with the lumped capacitors to periodically load a uniform TEM transmission line. The shorted length of line resonates the average value of the shunt capacitor at 815 mc.

The TEM transmission line chosen for this amplifier consists of a small round wire over a ground plane. The ground plane allows convenient access to one end of the crystal diodes to build an RF bypass network so that dc bias can be applied to each diode individually. The spacing of the wire over the ground plane, $h = 0.308$ inch, was determined by the length of the ceramic insulation in the diode cartridge. The characteristic impedance was then determined by the choice of wire size, $d = 0.010$ inch, the smallest practical size that could be easily handled. For the geometry shown in Fig. 4 this gives[22]

$$Z_0 = 285.4 \text{ ohms},$$

which will be the value used in all subsequent calculations.

The ω vs β curve is plotted in Fig. 5 along with the position of the pump signal at 1500 mc, and the other important frequencies associated with the amplifier. The straight line with 45-degree slope represents the ω vs β characteristic of the unperturbed TEM line.

In this particular structure, the ω vs β curve passes through the degenerate frequency point, 750 mc, as shown in Fig. 5, permitting the maximum possible gain for 750 mc since (2) is satisfied exactly. At other frequencies, the phase errors that are introduced reduce the gain as the edges of the band are approached. This tends to compensate for the fact that the image impedances increase towards the edges of the band, causing the gain to increase.

It should be pointed out that the pump frequency should not be phased so that it lies on the lines $\beta = n\pi$, $n = 0, 1, 2, \cdots$. If it did, the amplifier would have the same gain in both the forward and the backward directions, eliminating one of the principal advantages of the traveling-wave parametric amplifier, namely, unilateral amplification. The placement of the pump frequency as shown in Fig. 5 ensures that an adequate phase error exists between the pump wave and the backward waves on the amplifier so that a relatively small amount of interaction will occur.

Note also from Fig. 5 that the upper sideband frequencies are either in a stopband of the periodically loaded line or are grossly misphased with respect to the pump signal, so that no appreciable interaction will take place.

The maximum gain that can be obtained from this structure is given by (3). This maximum total gain for an eight-section amplifier (assuming that there are no phase errors and that the structure is terminated in its image impedance) is shown in Fig. 6 for several values of the peak capacitance variation, ΔC.

The RF bypass networks, which allow individual dc bias to be applied to each diode separately, consist of a

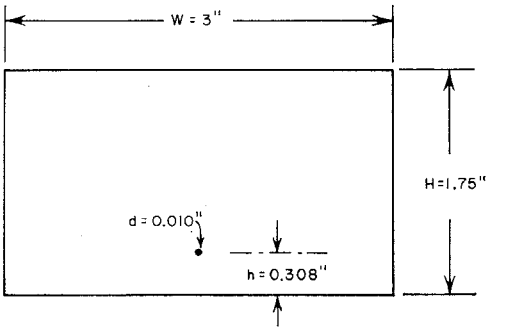

Fig. 4—Actual geometry of uniform transmission line.

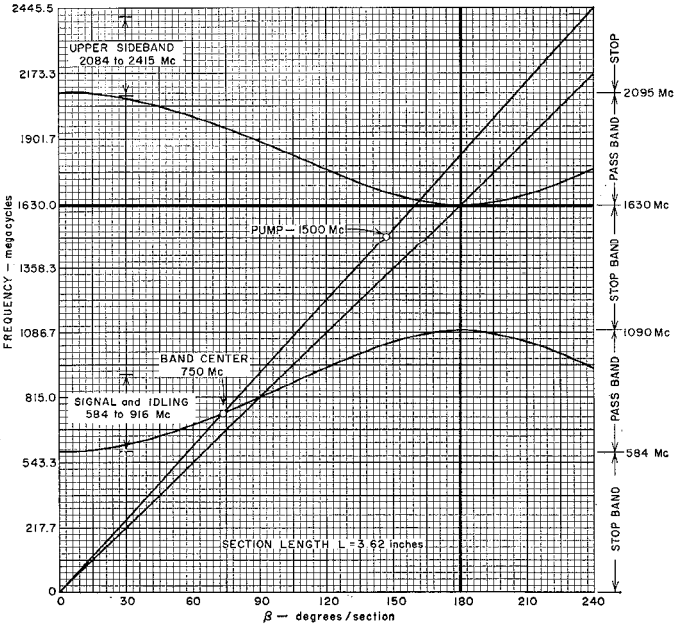

Fig. 5—ω vs β diagram for complete amplifier.

[22] "Reference Data for Radio Engineers," Federal Telegraph and Telephone Corp., New York N. Y., 4th ed., p. 593; 1956.

single π-section low-pass filter. The shunt capacitors are simply radial-line capacitors with thin mica dielectric, and the series inductance is a half-inch length of very high impedance coaxial line. No RF leakage could be detected past these filters, and no appreciable losses in the RF circuitry could be attributed to them.

Matching Networks

The purpose of the matching transformers shown in Fig. 1 is simply to transform the high image impedance of the amplifier down to a 50-ohm level for use with conventional coaxial instrumentation, and to terminate each end of the amplifier with impedances that are as close as possible to the image impedance of the amplifier. The π-section image impedance is much more constant over the signal band than the T-section image impedance. Therefore, an extra section was added to each end of the amplifier as shown in Fig. 7 so that the matching transformers could look into this π-section impedance. An average value of the π-section image impedance was then selected (336 ohms in this case) and an optimally designed stepped-transmission-line transformer[23] was used to match from 50 ohms into 336 ohms. This design used two intermediate quarter-wave sections ($n=3$) for a design bandwidth of 1.4 to 1. The end sections and matching transformers are shown with their important dimensions in Fig. 7.

The resultant over-all measured VSWR looking into the amplifier when it is terminated in a matched 50-ohm load is below 1.5:1 from 650 to 900 mc, and below 2:1 from 610 to 960 mc. The VSWR rises rapidly outside this band as the cutoff frequencies are approached.

In practice it was found that optimum performance was obtained if the networks were slightly modified by removing the parallel inductances adjacent to the amplifier terminals and the fixed capacitors at these terminals were replaced with variable capacitors that could be adjusted externally. These changes slightly improved the matches looking into the amplifier, keeping the measured input VSWR below 2:1 from 620 to 1020 mc.

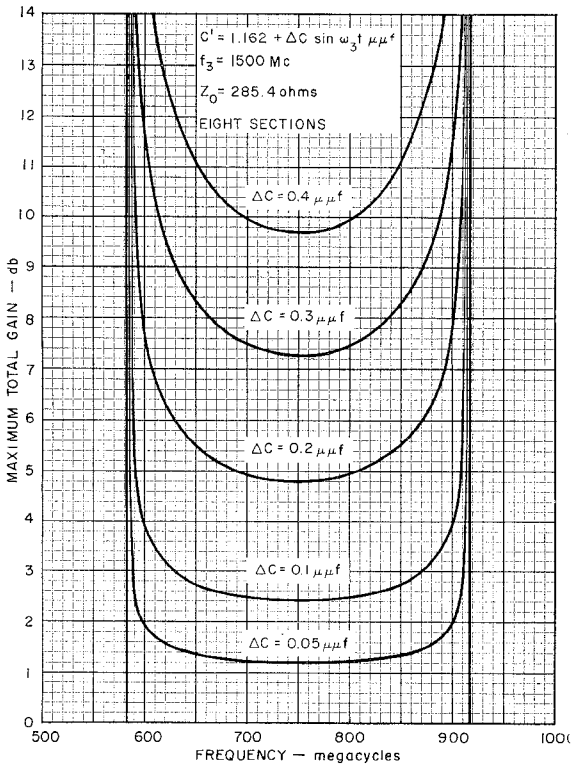

Fig. 6—Theoretical maximum total gain vs frequency.

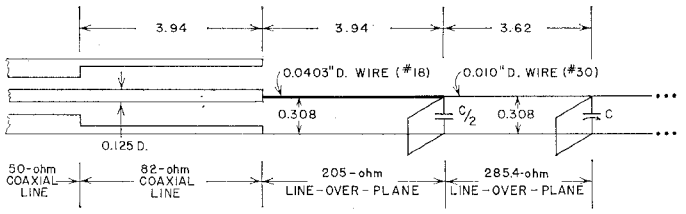

Fig. 7—Matching networks.

Test Cavity

In general, the available crystal diodes are not identical, and significant differences occur from diode to diode. Therefore, it was decided to test each diode individually in a separate cavity before installing it in the traveling-wave amplifier. This test cavity consisted of a length of transmission line with the same geometry as that in the parametric amplifier (Fig. 4). The length of the cavity was chosen to be one-half wavelength long at the resonant frequency of the shunt circuit, 815 mc. At the center of this cavity, the diodes could be mounted in shunt across the transmission line in exactly the same manner as in the amplifier. The cavity was used as a transmission cavity, with very loose loop coupling at each end of the cavity to keep the insertion loss greater than 40 db for all measurements. With no diode or diode mount in place, the cavity resonates at 815 mc. With a diode in place, the resonant frequency was lowered due to the shunt capacitance of the diode and its mount. By measuring this frequency, the total effective capacitance can be very accurately determined as a function of the external bias, and by measuring the Q of the resonance, the losses in the diode and the RF bypass filter can be inferred.

The reduction in the resonant frequency due to a lumped capacitor at the center of the cavity can be simply calculated in the following way. At resonance, the sum of the admittances looking in either direction from the center equals zero; therefore

$$j\frac{B}{2} - jY_0 \cot\frac{\beta_0 \ell}{2} = 0, \tag{10}$$

[23] S. B. Cohn, "Optimum design of stepped transmission-line transformers," IRE TRANS. ON MICROWAVE THEORY AND TECHNIQUES, vol. 3, pp. 16–21; April, 1955.

where, for this case,

$B=\omega C$, the susceptance of the lumped capacitance
$Y_0=1/Z_0$
$Z_0=285.4$ ohms, the characteristic impedance of the transmission line
$\beta_0=\omega/v=$ the phase constant of the unloaded transmission line
$\mathfrak{L}=7.23$ inches, the length of the cavity ($\lambda/2$ at 815 mc).

Hence, the shunt capacitance can be found as a function of frequency from

$$C=\frac{2Y_0}{\omega}\cot\frac{\beta_0\mathfrak{L}}{2}=\frac{2Y_0}{\omega}\cot\frac{\omega\mathfrak{L}}{2v}. \tag{11}$$

The Q's of the diodes, Q_d, can also be found from the Q's of the cavity plus diode, Q_0, from

$$Q_d=2Q_0\left(1+\frac{\beta_0\mathfrak{L}}{\sin\beta_0\mathfrak{L}}\right)^{-1} \tag{12}$$

assuming that the losses in the cavity are negligible compared to the losses in the diodes.[24]

After measuring the effective capacities and Q's of each diode as a function of bias, a length of transmission line (perpendicular to the main transmission line) was connected in parallel with the diode. This added line has a short circuit that can be adjusted to couple the desired inductive reactance across the diode. The position of this short circuit was adjusted until the cavity again resonated at 815 mc, at which frequency the parallel combination of short-circuited line plus diode and mount were also in resonance, resulting in a high resistive load across the transmission line in the cavity at the resonant frequency. The lengths of short-circuited line required to resonate each diode at a given bias were carefully measured, and the short circuits in the traveling-wave amplifier were adjusted to the same values.

Theoretical Noise Figure

Without Dissipation Loss: When a signal of frequency f_1 is applied to the input of a traveling-wave variable-reactance amplifier, the signal increases in amplitude as it travels down the length of the amplifier. At each diode the signal frequency, f_1, mixes with the pump frequency, f_3, and generates two principal sidebands at f_3+f_1 and f_3-f_1. The power in the lower sideband, or idling frequency, at $f_2=f_3-f_1$ also increases as it travels down the amplifier, while the power in the upper sideband interferes destructively at each diode.

If a current of amplitude a is applied to the left-hand, or input, end of the amplifier, one finds that the current on the transmission line to the right of the nth diode is given approximately by

$$I_1(n,t)=a\cosh(n\alpha)e^{j[2\pi f_1 t-(n-1)\beta_1]}. \tag{13}$$

Similarly, the current at the idling frequency f_2 just to the right of the nth diode is[25]

$$I_1^*(n,t)=\sqrt{\frac{f_2}{f_1}\frac{Z_{\pi 1}}{Z_{\pi 2}}}\,a\sinh(n\alpha)e^{j[2\pi f_2 t-(n-1)\beta_2]}. \tag{14}$$

In (14) the symbol * means complex conjugate. If one applies a current of amplitude a and frequency f_2 to the input, the currents to the right of each diode at frequencies f_1 and f_2 are determined by interchanging the subscripts in (13) and (14).

If a matched noise generator, having available noise power kT_1B at $T_1°$ K whose noise spectrum is centered about f_1, is connected to the input of the amplifier, it is clear that

$$kT_1B=I_1I_1^*Z_{\pi 1}=a^2Z_{\pi 1} \tag{15}$$

where Boltzmann's constant $k=1.38\times10^{-23}$ watt-seconds per degree Kelvin. Hence the noise power $N_1'(n)$ in the bandwidth B centered at f_1 to the right of the nth diode becomes

$$N_1'(n)=kT_1B\cosh^2(n\alpha), \tag{16}$$

while the noise power, $N_2'(n)$ in the bandwidth B centered at f_2 to the right of the nth diode becomes

$$N_2'(n)=kT_1B\frac{f_2}{f_1}\sinh^2(n\alpha). \tag{17}$$

Similar expressions are obtained when a matched generator at temperature T_2 having available noise power kT_2B, whose noise spectrum is centered about f_2, is connected to the input of the amplifier. Then the noise power, $N_1''(n)$, in the bandwidth, B, centered about f_1 to the right of the nth diode is

$$N_1''(n)=kT_2B\frac{f_1}{f_2}\sinh^2(n\alpha), \tag{18}$$

while the noise power, $N_2''(n)$, in the bandwidth, B, centered at f_2 becomes

$$N_2''(n)=kT_2\cosh^2(n\alpha). \tag{19}$$

Therefore, the total noise powers out of the signal and idling frequency channels are given, respectively, by

$$N_1(n)=N_1'(n)+N_1''(n)=kB\left[T_1\cosh^2(n\alpha)+T_2\frac{f_1}{f_2}\sinh^2(n\alpha)\right] \tag{20}$$

[24] E. M. T. Jones, G. L. Matthaei, S. B. Cohn, and B. M. Schiffman, "Design Criteria for Microwave Filters and Coupling Structures," Stanford Res. Inst., Menlo Park, Calif., Tech. Rept. 5, Contract DA 36-039 SC-74862, pp. 5–11; March, 1959.

[25] Eqs. (13) and (14) are obtained in an obvious way from (27) and (28) of Tien and Suhl, *op. cit.*

$$N_2(n) = N_2'(n) + N_2''(n)$$
$$= kB\left[T_2 \cosh^2(n\alpha) + T_1 \frac{f_2}{f_1} \sinh^2(n\alpha)\right]. \quad (21)$$

Eqs. (20) and (21) can also be applied to signals of power P_1 in Channel 1 and P_2 in Channel 2, in which case the output signal powers in the two channels are given by

$$S_1(n) = P_1 \cosh^2(n\alpha) + P_2 \frac{f_1}{f_2} \sinh^2(n\alpha) \quad (22)$$

$$S_2(n) = P_2 \cosh^2(n\alpha) + P_1 \frac{f_2}{f_1} \sinh^2(n\alpha). \quad (23)$$

The noise figure of an amplifier is defined by

$$F = \frac{N_{\text{out}}}{N_{\text{in}}} \cdot \frac{S_{\text{in}}}{S_{\text{out}}} \quad (24)$$

where N_{in} is the available input thermal-noise power from the generator resistance (at a temperature $T_1 = 290°\text{K}$ by convention) in the band around the signal frequency, N_{out} is the available output noise power, S_{in} is the available input signal power from the generator, and S_{out} is the available output signal power. $S_{\text{out}}/S_{\text{in}}$ may be defined as the power gain of the amplifier. Because of the multiplicity of channels that must be considered in amplifiers such as this, several different modes of operation can be visualized which may have different *effective* noise figures.

These different modes can be treated as follows, using (20) to (24):

Case I—Input signal on Channel 1 only; output detected on Channel 1 only.

$$(P_2 = 0,\ T_1 = 290°\text{K})$$
$$F_{\text{I}} = \frac{N_1(n)}{k290B} \cdot \frac{P_1}{S_1(n)}$$
$$= 1 + \frac{T_2}{290} \frac{f_1}{f_2} \tanh^2(n\alpha)$$
$$\approx 1 + \frac{T_2}{290} \frac{f_1}{f_2} \text{ for large gain } (n\alpha > 2). \quad (25)$$

This case corresponds to the most usual manner for using these amplifiers with single-frequency signals, and the noise figure so found corresponds to the IRE definition of noise figure.[26] The manner in which this noise figure varies with gain is illustrated in Fig. 8.

Case II—Input signal on Channel 1 only; output detected on Channel 2 only.

$$(P_2 = 0,\ T_1 = 290°\text{K})$$

[26] "Standards on Receivers: Definitions of Terms, 1952," PROC. IRE, vol. 40, pp. 1681–1685; December, 1952.

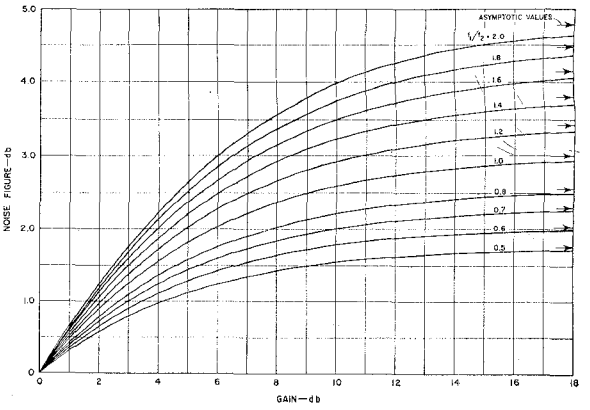

Fig. 8—Noise figure vs signal gain.

$$F_{\text{II}} = \frac{N_2(n)}{k290B} \cdot \frac{P_1}{S_2(n)}$$
$$= 1 + \frac{T_2}{290} \frac{f_1}{f_2} \coth^2(n\alpha)$$
$$\approx 1 + \frac{T_2}{290} \frac{f_1}{f_2} \text{ for large gain } (n\alpha > 2). \quad (26)$$

This case is always worse than Case I, although they approach each other for high gain. Again, the IRE definition of noise figure agrees with this definition.

Case III—Input signal on Channel 1 only; output detected on Channels 1 and 2.

$$(P_2 = 0,\ T_1 = 290°\text{K})$$
$$F_{\text{III}} = \frac{N_1(n) + N_2(n)}{k290B} \cdot \frac{P_1}{S_1(n) + S_2(n)}$$
$$= 1 + \frac{T_2}{290} \frac{1 + \frac{f_1}{f_2} \tanh^2(n\alpha)}{1 + \frac{f_2}{f_1} \tanh^2(n\alpha)}$$
$$\approx 1 + \frac{T_2}{290} \cdot \frac{f_1}{f_2} \text{ for large gain } (n\alpha > 2). \quad (27)$$

There are regions in which Case III will yield a lower noise figure than Case I, and others where it will be higher, although they approach each other for high gain.

Case IV—Uncorrelated input signals on Channels 1 and 2; output detected on Channel 1 only.

$$(P_1 = P_2 = P,\ T_1 = T_2 = 290°\text{K})$$
$$F_{\text{IV}} = \frac{N_1(n)}{2k290B} \cdot \frac{2P}{S_1(n)} = 1. \quad (28)$$

Case V—Uncorrelated input signals on Channels 1 and 2; output detected on Channels 1 and 2.

$$(P_1 = P_2 = P,\ T_1 = T_2 = 290°\text{K})$$

$$F_V = \frac{N_1(n) + N_2(n)}{2 \times k290B} \cdot \frac{2P}{S_1(n) + S_2(n)} = 1. \quad (29)$$

This case and Case IV correspond to the usual manner for using these amplifiers with broad-band noise signals, such as in many radio astronomy applications and in measuring the noise figures of these amplifiers with broad-band gas-discharge, noise sources. Case V also corresponds to the use of these amplifiers around the degenerate frequency by considering that the total bandwith B' of the amplifier is divided into a bandwidth B just below the degenerate frequency, $f_2/2$, and an equal bandwidth B just above the degenerate frequency.

Case VI—Correlated input signals on Channels 1 and 2; output detected on Channels 1 and 2; degenerate case.

($f_1 = f_2$ and phased so that signal voltages add)

$$(P_1 = P_2 = P,\ T_1 = T_2 = 290°\text{K})$$

$$F_{VI} = \frac{N_1(n) + N_2(n)}{2 \times k290B} \cdot \frac{2P}{[\sqrt{S_1(n)} + \sqrt{S_2(n)}]^2} = \frac{1}{2}. \quad (30)$$

This rather surprising answer[27] results from the fact that the phase of the signal has been assumed to be locked to the phase of the pump in such a way that maximum gain occurs, *i.e.*, that more information (phase information) is required to make this system work.

With Dissipation Loss: In approximating the noise figure of an n-section traveling-wave variable-reactance amplifier whose diodes have dissipation loss, it is convenient to consider the amplifier as a cascade of n amplifiers with noise figures, F_n, and cold insertion losses, L_n. If the input and output bandwidths include both signal and idle channels (Case V), the over-all noise figure of the complete amplifier, F_V, can be found from the total output noise power

$$\begin{aligned} N_{out} &= k290B\left[\cosh^2(n\alpha) + \frac{1}{2}\left(\frac{f_1}{f_2} + \frac{f_2}{f_1}\right)\sinh^2(n\alpha)\right]F_V \\ &= k290B\left\{F_1\left[\cosh^2(n\alpha) + \frac{1}{2}\left(\frac{f_1}{f_2} + \frac{f_2}{f_1}\right)\sinh^2(n\alpha)\right]\right. \\ &+ (F_2 - 1)\left[\cosh^2(n-1)\alpha\right. \\ &\quad \left. + \frac{1}{2}\left(\frac{f_1}{f_2} + \frac{f_2}{f_1}\right)\sinh^2(n-1)\alpha\right] + \cdots \\ &+ (F_n - 1)\left[\cosh^2\alpha\right. \\ &\quad \left.\left. + \frac{1}{2}\left(\frac{f_1}{f_2} + \frac{f_2}{f_1}\right)\sinh^2\alpha\right]\right\}, \end{aligned} \quad (31)$$

where the α's are computed from the total net gain of the amplifier,

$$\cosh^2(n\alpha) + \frac{1}{2}\left(\frac{f_1}{f_2} + \frac{f_2}{f_1}\right)\sinh^2(n\alpha). \quad (32)$$

If one operates the amplifier in the vicinity of the degenerate frequency, so that $f_1 \approx f_2$, then (31) reduces to the simpler expression

$$\begin{aligned} F_V - 1 &= (F_1 - 1) + (F_2 - 1)\frac{\cosh 2(n-1)\alpha}{\cosh 2n\alpha} \\ &+ \cdots + (F_n - 1)\frac{\cosh 2\alpha}{\cosh 2n\alpha} \end{aligned} \quad (33)$$

where the α's are computed from the total *net* gain of the amplifier,

$$\cosh^2 n\alpha + \sinh^2 n\alpha = \cosh(2n\alpha). \quad (34)$$

These expressions differ from the usual cascaded-amplifier noise figure expressions since the gain of any given stage for uncorrelated noise generated within itself is, in general, less than its gain for the correlated noise and signals received from the previous stage.

Assuming that the losses are the same at f_1 and f_2, the noise figure of each stage, F_n, is approximately equal to its insertion loss, L_n, for small gain per stage. Since the losses in each stage are also assumed to be equal,

$$L_1 = L_2 = \cdots = L_n = L^{1/n},$$

where L is the total insertion loss in the amplifier expressed as a power ratio ≥ 1. Therefore, the total excess noise from the amplifier operated near the degenerate frequency is given by

$$\begin{aligned} F_V - 1 = \frac{L^{1/n} - 1}{\cosh 2n\alpha}&[\cosh 2n\alpha + \cosh 2(n-1)\alpha \\ &+ \cdots + \cosh 2\alpha]. \end{aligned} \quad (35)$$

Assuming that the noise in the output of the amplifier divides up in about the same way between the signal and idling channels in the lossy case as in the lossless case, the noise figure for single-channel operation (Case I) can be found from the double-channel operation case treated above by comparing (25) and (29) to give

$$F_I \approx F_V\left(1 + \frac{f_1}{f_2}\tanh^2 n\alpha\right) \quad (36)$$

where F_V can be found from (31).

Experimental Procedure and Results

Diodes in Test Cavity

A variety of diodes were checked in the test cavity described in the previous section. The eight diodes chosen for the tests of the traveling-wave parametric amplifier were selected from a group of diffused-junction silicon diodes from Microwave Associates, Inc., and Bell Telephone Laboratories. The total effective capaci-

[27] S. B. Cohn, "The noise figure muddle," *Microwave J.*, vol. 2, pp. 7–11; March, 1959.

ties of these diodes plus their mounts as a function of external dc bias are shown in Fig. 9.

An inductance consisting of a length of short-circuited transmission line was then connected in parallel with each diode and adjusted as described previously. The final over-all Q_0's of the test cavity with diodes and short-circuited lines varied from 90 to 120. Assuming that all of the losses occur in the series resistance of the diodes, the actual Q of the diodes, Q_d, can be found from (12), giving Q_d's around 50.

Amplifier

Operation: A photograph of the amplifier is shown in Fig. 10. The variable-width pump waveguide loaded with a $1\frac{1}{4}$-inch-diameter polystyrene rod placed on top of a $1\frac{1}{2}$-inch-high by 1-inch-wide metal ridge is seen on the left. This composite loading structure was used in order to achieve the proper phase velocity of the 1500-mc TE_{10} mode in the pump waveguide and at the same time to suppress in the pump waveguide the TE_{20} mode of propagation at the pump frequency of 1500 mc and to suppress the TE_{10} mode of propagation in the pump waveguide at 916 mc, the highest signal or idling frequency. The waveguide and the adjustable probes coupling to each diode are also evident in the photograph. The matching networks can be seen at either end of the amplifier. The RF bypass networks are contained in the structure along the right edge of the amplifier. External to these bypass networks, a 1000-micromicrofarad condenser and a 5-megohm variable resistance were connected to ground across each diode. The resistors provide dc return paths for the diodes, and a resistance across which self-bias voltage can be developed. The capacitors provide some measure of protection for the diodes from static discharges and other external transients that might damage them.

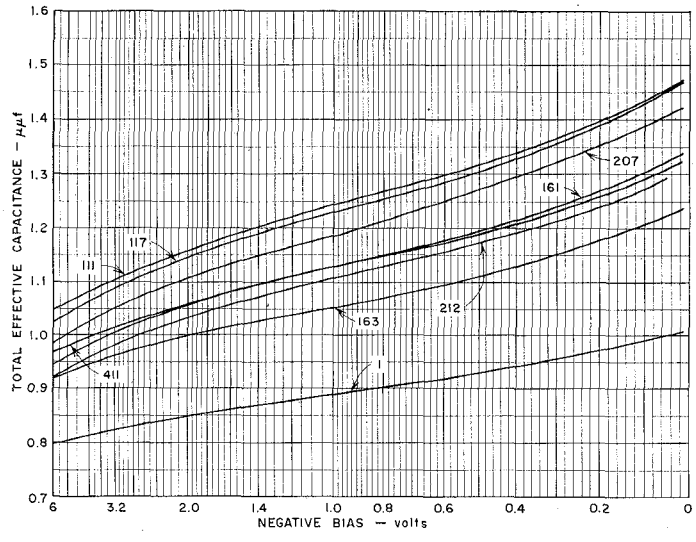

Fig. 9—Total capacitance vs bias.

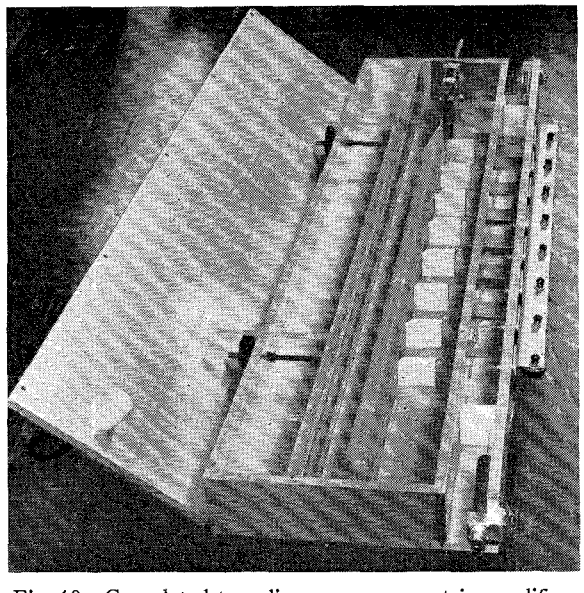

Fig. 10—Completed traveling-wave parametric amplifier.

The procedure for tuning up this amplifier was as follows. First, the couplings from the pump waveguide to each diode were adjusted so that the loop sizes and the gaps forming the capacitive couplings to each diode were all mechanically identical. Then, the individual bias resistors connected across each diode were adjusted to provide optimum performance without oscillation anywhere in the band.

The 1500-mc CW pump power was supplied by an Airborne Instruments Laboratory Model 124A Power Oscillator followed by suitable filters, providing at least 10 watts of pump power to the pump waveguide when required. Only a very small fraction of this total power was coupled out to the diodes, so that the actual pump power required by the amplifier could not be readily measured.

Normally, the amplifier was fed from a well-padded 1000-cycle-modulated signal generator at sufficiently low signal levels that the self-bias voltages were not affected by the signal even in regions of high gain. The amplifier was terminated with a large, well-matched attenuator followed by a low-pass filter that passed the signal and idling frequencies but was cut off to the pump frequency. Both the signal and the idling frequencies were detected simultaneously with a matched broadband detector feeding a narrow-band 1000-cycle amplifier.

The input signal generator was mechanically swept over the band from about 500 mc to 930 mc in synchronism with the horizontal sweep of an oscilloscope with a long-persistence screen. The output from the square-law detector was fed to the vertical deflection plates, and a continuous plot of total output power vs frequency was obtained on the oscilloscope. It was then a very simple matter to make adjustments to the amplifier and observe their effects everywhere in the band. When a good combination of the various parameters was found, a photograph of the trace on the oscilloscope recorded all the data. These photographs, combined with similar traces of the output of the detector when

the pump signal was removed, and also when the amplifier was bypassed, were sufficient to provide a fairly complete picture of the amplifier performance. Point-by-point measurements were also taken of a few of the better operating points to check the photographic data.

Gain: The final adjustments to the amplifier to obtain optimum response yielded the experimental results shown by the solid curves in Fig. 11. Because of the relatively high losses in the diodes, the cold insertion loss of the amplifier was about 3 db or more over most of the band. To measure the cold insertion loss, the external bias voltage applied to the diodes was set equal to the self-bias voltage on the diodes when they are being pumped. This high insertion loss limited the net signal gain that could be obtained from the amplifier to a minimum of about 4 db over most of the band. Attempts to increase this gain at the middle of the band only resulted in oscillation at the edges of the band where the gain is very high due to the high image impedances and regeneration within the amplifier.

The solid curves in Fig. 11 are the output of the broad-band detector, corresponding to the sum of the signal and idling frequency powers. Since, in general, these two powers are not equal, the gain in the signal channel alone can be calculated approximately in the following way. As shown previously, the power in the signal channel increases as $\cosh^2(n\alpha)$ along the amplifier, and in the idling channel as $(f_2/f_1)\sinh^2(n\alpha)$. The sum of these powers is then proportional to

$$P_T = \cosh^2(n\alpha) + \frac{f_2}{f_1}\sinh^2(n\alpha)$$

which is the quantity measured by the broad-band detector assuming that it is equally sensitive to the powers at the two frequencies. This quantity is always greater than the power in the signal channel alone by the ratio

$$R = \frac{P_T}{P_S} = \frac{\cosh^2(n\alpha) + \frac{f_2}{f_1}\sinh^2(n\alpha)}{\cosh^2(n\alpha)}$$

$$= 1 + \frac{f_2}{f_1}\tanh^2(n\alpha). \tag{37}$$

Thus, knowing the frequency ratio, f_2/f_1, and the total gain, the signal gain can be determined. This calculation has been applied to the data in Fig. 11 and the results are shown by the dashed curves in the figure.

It is apparent, however, that in certain applications, over-all system performance could be significantly improved by detecting both the signal and the idling frequency powers.

Noise Figure: The noise figure of the amplifier was measured using wideband noise generated by a gas-discharge noise source and fed into both the signal and the idling channels on each side of the degenerate frequency, $f_3/2$. The output of the amplifier in the band around the degenerate frequency was fed to a crystal-mixer, through a 30-mc IF amplifier to a Hewlett-Packard noise-figure meter that automatically computes the noise figure from the ratio of the signal it receives when the noise tube is on to the signal it receives when the noise tube is off.

The complete block diagram of the experimental equipment used to measure this noise figure near the degenerate frequency (750 mc) is shown in Fig. 12. The noise figure of the amplifier alone is computed in the usual way,

$$F_1 = F - \frac{F_2 - 1}{G_1} \tag{38}$$

where F_1 and G_1 are the noise figure and the power gain of the parametric amplifier, F_2 is the measured noise figure of the second stage, and F is the measured over-all noise figure of both stages. These noise figures correspond to those already defined in Case V.

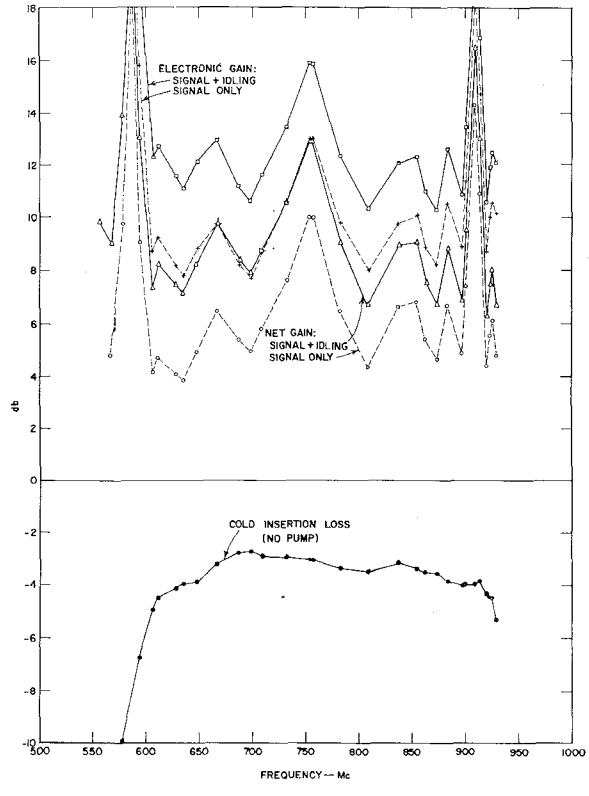

Fig. 11—Performance of amplifier.

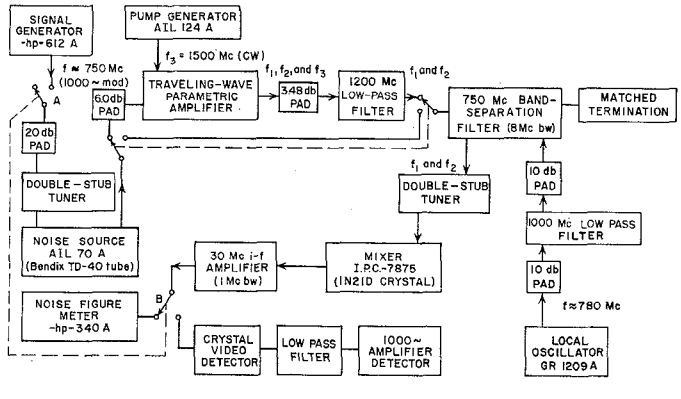

Fig. 12—Experimental setup for measuring noise figures.

The strip-line band-separation filter included in Fig. 12 was built to use in measuring the noise figure and is of the type shown in Fig. 3(e) in Cohn and Coale.[28] This type of filter has the advantage that it appears well-matched to the amplifier at all frequencies, thus greatly reducing the regeneration within the amplifier, yet it diverts an 8-mc band around the degenerate frequency from the output of the amplifier into the second stage. Furthermore, it provides a convenient means of introducing the local-oscillator signal into the crystal mixer as shown in the figure.

In using the gas-discharge noise source, and applying (38), a number of precautions must be taken to ensure accurate results. These precautions include such things as:

1) Corrections of the noise-figure readings due to the difference between the actual excess noise figure of the gas tube and its rated value of 15.2 db due to incomplete coupling (determined from its hot insertion loss at 750 mc, 22.4 db) and internal losses (determined from its cold insertion loss at 750 mc, 0.75 db).[29] For this particular tube at 750 mc this amounts to 0.35 db subtracted from all noise-figure meter readings.
2) Accurately measuring and accounting for all losses in the pads and cables used in the measuring set-up.
3) Ensuring that the output impedance of the noise source is exactly the same whether the tube is off or on. If this impedance were to change, it would change the phase or amplitude of any reflection from the noise source, hence changing the regeneration and the gain within the amplifier due to these small reflections. This is the purpose of the double stub tuner preceding the noise source shown in Fig. 12. The pads at the inputs to each amplifier also help to reduce this effect.
4) Ensuring that the temperature of the gas discharge tube does not rise sufficiently far above 290°K during operation to appreciably alter the noise from the source when the gas discharge is off. This noise is a function of both the temperature of the pad preceding the noise source and the cold insertion loss of the tube.

After taking all of these precautions, and adjusting the amplifier until everything was stable, a series of noise-figure measurements were made for frequencies very close to the degenerate frequency, $f_3/2$. The results of these measurements are shown in Table I, under the heading "Amplifier 2" along with theoretical values calculated from (34) to (36). The results in Table I for Amplifier 1 were obtained on an amplifier similar to the one described that had a higher cold insertion loss and less over-all gain. The measured values of F_V, the effective noise figures for wideband noise inputs are about 1.2 db higher than the calculated values for both amplifiers. This may be due to a variety of causes, some of which are:

1) Change in the insertion loss of the amplifiers with pumping due to an increase in the average value of the capacitances of the diodes.
2) Inaccurate calibration of the excess noise from the cold-cathode gas discharge noise source.
3) An accumulation of small errors due to the various sources of experimental error listed above.
4) Noise from the pump generator.
5) Small instabilities in the amplifier due to small changes in the pump power and signal level and even small thermal changes.

Note that the theoretical values of noise figures will decrease as the gain of the amplifiers increases. For Amplifier 2, with 3-db cold loss, F_V approaches 0.4 db and F_I approaches 3.4 db as the gain of the amplifier approaches infinity.

TABLE I
EXPERIMENTAL AND THEORETICAL NOISE FIGURES

Amplifier	Net Gain (Signal plus Idling)	Cold Loss	Measured Noise Figure F_V		Theoretical Noise Figures	
			Maximum Limits	Average	F_V (noise)	F_I (sig. gen.)
1	5.25 db	4.3 db	3.10–3.33 db	3.25 db	2.00 db	3.88 db
2	9.5 db	3.0 db	2.26–2.36 db	2.32 db	1.11 db	3.66 db

CONCLUSIONS

The traveling-wave parametric amplifiers described operate in the manner predicted theoretically, indicating that the techniques developed for their design are useful and valid. The particular type of amplifier built is limited in its usefulness by two principal factors: 1) the high gain at the edges of the pass band due to the high image impedance of the periodically loaded structure, and 2) the ripples in the pass band when high gain is required that are caused by small reflections from the amplifier terminations and some interaction with the backward waves. The introduction of nonreciprocal or even reciprocal loss can alleviate both of these problems. Alternative circuits with image impedances approaching zero at the edge of the band would eliminate the first difficulty. It may also be possible to synthesize nonperiodic filter structures which would avoid both of the above problems.

[28] S. B. Cohn and F. S. Coale, "Directional channel-separation filters," PROC. IRE, vol. 44, pp. 1018–1024; August, 1956.
[29] J. S. Honda and E. D. Sharp, "Investigation of Methods of Scanning the Beam of Large Antennas," Stanford Res. Inst., Menlo Park, Calif., Scientific Report 8, Contract AF 19(604)-2240; June, 1959.